**NASA TECHNICAL MEMORANDUM**

NASA TM-73838



NASA TM-73838

# AN EMPIRICAL MODEL FOR INVERTED-VELOCITY-PROFILE JET NOISE PREDICTION

by James R. Stone
Lewis Research Center
Cleveland, Ohio 44135

TECHNICAL PAPER to be presented at the
Ninety-fourth Meeting of the
Acoustical Society of America
Miami, Florida, December 13-16, 1977

# AN EMPIRICAL MODEL FOR INVERTED-VELOCITY-PROFILE JET NOISE PREDICTION

by James R. Stone

National Aeronautics and Space Administration
Lewis Research Center
Cleveland, Ohio 44135

E-9425

## ABSTRACT

An empirical model for predicting the noise from inverted-velocity-profile coaxial or coannular jets is presented and compared with small-scale static and simulated-flight data. The model considers the combined contributions of as many as four uncorrelated constituent sources: the premerged-jet/ambient mixing region, the merged-jet/ambient mixing region, outer-stream shock/turbulence interaction, and inner-stream shock/turbulence interaction. The model for both mixing regions is developed from the NASA interim prediction method for jet noise. The noise from the merged region occurs at relative low frequency and is modelled as the contribution of a circular jet at merged conditions (between inner and outer streams) and total exhaust area, with the high frequencies attenuated (since the high frequency region of this fictitious jet does not exist). The noise from the premerged region occurs at higher frequency and is modelled as the contribution of an equivalent plug nozzle at outer stream conditions, with the low frequencies attenuated (since the outer jet is broken up rapidly, before much low frequency is generated). The shock noise for each supersonic stream is calculated from a modification of the Harper-Bourne and Fisher (1973) model.

STAR Category 71

## INTRODUCTION

The development of an environmentally and economically acceptable advanced supersonic aircraft will require substantial advancements in noise technology compared to the current, first-generation supersonic aircraft. Inverted-velocity-profile coaxial and coannular nozzles have been identified as a major breakthrough in jet noise suppression applicable to supersonic aircraft engines (e.g., ref. 1). The aero/acoustic benefits associated with inverted-velocity-profile jets were first identified in a series of tests under NASA Lewis Research Center sponsorship (refs. 2-4). In order to perform engine/aircraft tradeoff studies to identify the most promising designs, it is necessary to be able to predict the acoustic performance of these nozzles. This paper presents an empirical model for making such predictions.

It has been recognized (e.g., refs. 4-5) that the noise generated by inverted-velocity-profile jets should be modeled as the combined contributions of various source regions and noise generation mechanisms. The model presented in this paper considers the noise generated by two jet-mixing regions and two potential regions of shock/turbulence interaction. The noise prediction models for both jet-mixing regions are developed from the NASA interim prediction method for jet noise (ref. 6), and the shock/turbulence interaction noise predictions are based on modification of the Harper-Bourne and Fisher model (ref. 7). Possible noise benefits due to shock interactions when both streams are supersonic, such as described by Dosanjh, et al. (e.g., ref. 8), are not included in the present method. Instead, the two streams are considered to generate shock noise independently.

The jet-mixing noise is considered to emanate from two regions: a premerged region, where the individual jets are identifiable, and a merged region. Equivalent single jets are hypothesized to approximate these regions. But then the low-frequency premerged noise must be reduced ("cut-off") to account for the fact

that the premerged region does not exist far enough downstream for much low-frequency noise to be generated, and the high-frequency merged noise must be reduced (cut-off) since the high-frequency noise generating region of the hypothetical jet does not exist. Similar reasoning has been applied to premerged-region noise generated for multitube suppressor nozzles (e.g., ref. 9).

Results calculated from the empirical model presented herein are compared with model-scale experimental data for static (refs. 2-3) and simulated flight (ref. 10) conditions. These comparisons are made for cases where both streams are subsonic, where the outer stream is supersonic with the inner stream subsonic, and where both streams are supersonic. The cases considered cover a range of inner-to-outer-stream area ratio and include both coaxial (without center plug) and coannular (with center plug) nozzles.

## DEVELOPMENT OF EMPIRICAL MODEL

The jet noise for an inverted-velocity-profile coaxial or coannular nozzle is considered to be made up of as many as four constituent sources, as illustrated in figure 1:

(1) Merged-jet/ambient mixing region (subscript m)

(2) Premerged-jet/ambient mixing region (subscript p)

(3) Inner-stream shock/turbulence interaction (subscript s, 1)

(4) Outer-stream shock/turbulence interaction (subscript s, 2)

The noises from all these sources are assumed to be uncorrelated, so that

$$SPL = 10 \log \left( 10^{SPL_m/10} + 10^{SPL_p/10} + 10^{SPL_{s,1}/10} + 10^{SPL_{s,2}/10} \right) \tag{1}$$

The methods of predicting these constituent spectral components are given in the following sections. The prediction methods are set

up to approach the single-jet case in the limit as $V_2 \rightarrow V_1$ and $T_2 \rightarrow T_1$. All symbols are defined in appendix A.

Experimental noise measurements are often made at a distance far enough from the sources to be in the acoustic far field, but not far enough away to treat the entire region as a point source (e.g., see ref. 11). When this is the case, the prediction for each source must take into account the location of that source. The methods used to approximate these source location effects are given in appendix B.

## Merged Jet Noise

The noise from the merged-jet ambient mixing region occurs at relatively low frequency and is usually the most important component in the full scale static overall sound pressure level, OASPL, and perceived noise level, PNL. The method of prediction, illustrated conceptually in figure 2, is to treat the merged-jet region as a circular jet at equivalent merged conditions (intermediate between inner and outer streams) and total exhaust area. However, the high frequency region is decreased (shaded region labeled "cutoff" in fig. 2) since the high frequency region of this fictitious jet does not exist. The equivalent circular jet noise ($SPL_j$) is computed herein from the NASA interim prediction method for jet noise (ref. 6) using as inputs the effective jet conditions defined in the following paragraph. However, the same basic approach could alternatively be used in conjunction with other circular jet noise predictions or with a reliable set of circular jet noise experimental data.

Effective jet conditions. - As illustrated in figure 2, the outer jet velocity, which is initially the peak velocity, decreases rapidly with downstream axial distance, while the centerline velocity first increases as momentum is transferred inward and then begins to decrease. At some point the centerline velocity becomes the peak

velocity; it is a velocity (and a temperature) in this region that should be used to characterize the merged-jet/ambient mixing region. The characteristic velocity and temperature (total) used herein are calculated from the following relations:[1]

$$V_m = \frac{V_1 + V_2\left(\frac{A_2}{A_1}\sqrt{\frac{T_1}{T_2}}\right)}{1 + \left(\frac{A_2}{A_1}\sqrt{\frac{T_1}{T_2}}\right)} \tag{2}$$

$$T_m = \frac{T_1 + T_2\left(\frac{A_2}{A_1}\sqrt{\frac{T_1}{T_2}}\right)}{1 + \left(\frac{A_2}{A_1}\sqrt{\frac{T_1}{T_2}}\right)} \tag{3}$$

The diameter used is the total equivalent diameter of the two streams,

$$D_m = \sqrt{\frac{4}{\pi}(A_1 + A_2)} \tag{4}$$

Cutoff. - To account for the fact that the high frequency region does not exist for this fictitious jet, a correction must be applied which is frequency dependent. (A similar, but reversed, correction is applied to the premerged noise, so that the proper single jet limit is approached when the two spectra are combined.) The simple approximate term used in the present study is given by

[1]Unpublished information obtained under NASA Lewis contract NAS3-20061, April 1977.

$$SPL_m = SPL_j - 10 \log\left[1 + \frac{fD_m}{V_m}\left(\frac{T_m}{T_a}\right)^{0.4}\right] \quad (5)$$

Flight effects. - The effects of flight on jet noise are evaluated herein by the method of reference 6 except for the kinematic term, which should be added:

$$SPL_f - SPL_{st} = -10 \log(1 - M_0 \cos \theta) \quad (6)$$

It should be noted that this kinematic term arises from relative motion between the source and the microphone. Thus, for free jet or wind tunnel flight simulation, this term from equation (6) is zero. The dynamic effect, included in reference 6, is based on the motion of the source relative to the propagation medium. These dynamic effects are included in the simulated flight case. In order to avoid ambiguity the terms, $M_0 = V_0/c_a$, and, $M_a = V_a/c_a$ are used. The velocity of the nozzle with respect to the microphone is denoted by $V_0$, and the velocity of the free stream with respect to the nozzle is denoted by $V_a$. (In flight over a stationary microphone, $V_0 = V_a$.)

## Premerged Jet Noise

The noise from the premerged-jet/ambient mixing region occurs at intermediate to high frequencies. Though it is usually less important than the merged noise for the full-scale case statically, in flight its importance may be enhanced, particularly with regard to the PNL. The method of prediction, illustrated conceptually in figure 3, is to treat the outer stream as if it were exhausting from a plug nozzle. However, the low frequency region is attenuated (shaded region labeled "cut-off" in fig. 3) since the outer jet decays rapidly with downstream axial distance, before

much low frequency noise is generated. The same circular jet noise prediction (ref. 6) is used as a starting point here as was used for the merged jet, but both frequency and level shifts are made to account for plug nozzle effects and interaction of the two streams.

Plug nozzle and interaction effects. - Plug nozzles have been found to produce somewhat less noise than circular nozzles of the same area, and such an effect was included in reference 6. More recent results (e.g., ref. 3) have indicated a stronger plug effect, and the presence of inner stream flow also has an effect, so a new relationship is needed. The following relationship, based on a modification to the reference 6 plug nozzle effect, is used in this paper:

$$SPL_{P1} = SPL_j + 5 \log \left[ 1 + 2\left(\frac{H_2}{D_2}\right)\left(1 - \frac{V_1}{V_2}\right) + 2\left(\frac{H_2 + H_1}{D_2}\right) \frac{(V_1/V_2)^{20}}{1 + (V_1/V_2)^{20}} \right] \tag{7}$$

(The term incorporating velocity ratio the twentieth power brings about approximately correct limiting behavior, recalling that the present method is limited to $V_2 > V_1$.) The plug nozzle noise is also shifted to higher frequency than the equivalent circular nozzle; the relationship of reference 6 is used for this effect,

$$f_p = f_j \left( \frac{A_2}{\pi H_2^2} \right)^{0.2} \tag{8}$$

Cutoff. - To account for the fact that the annular outer jet loses its identity before much noise is generated at low frequency, the following correction is applied:

$$SPL_p = SPL_{P1} - 10 \log \left[ 1 + \frac{V_2}{f(2H_2 + L_2)} \left( \frac{T_a}{T_2} \right)^{0.4} \right] \qquad (9)$$

Flight effects. - As was done for the merged noise, a kinematic term is added, as given by equation (6).

## Shock Noises

The shock noise, for each stream which is supersonic, is calculated separately. Thus, no accounting is made for interaction between the two streams or their shock structures. The peak sound pressure levels are computed from the following modifications to the Harper-Bourne and Fisher (ref. 7) method, based on a cursory evaluation of the data of references 2 and 3:

$$SPL_{s,1}^{peak} = 151 + 10 \log \left\{ \frac{\left[ 1 - 0.43 \left( \frac{D_1 - 2H_1}{D_1} \right)^2 \right]^4 \left( M_1^2 - 1 \right)^2}{(1 - M_a \cos \theta)^3 (1 - M_0 \cos \theta)} \right\}$$

$$+ 10 \log \left( \frac{A_1}{R^2} \right) \qquad (10a)$$

for the inner stream, and for the outer stream

$$SPL_{s,2}^{peak} = 151 + 10 \log\left(\frac{A_2}{R^2}\right) + 10 \log$$

$$\times \left\{ \frac{\left[1 - 0.43\left(\frac{D_2 - 2H_2}{D_2}\right)^2\right]^4 \left(M_2^2 - 1\right)^2}{(1 - M_a \cos\theta)^3 (1 - M_0 \cos\theta)} \right\} \qquad (10b)$$

The frequencies at which these peaks occur are given by

$$f_{s,1}^{peak} = 0.62\, V_1/(2H_1) \Big/ \sqrt{M_1^2 - 1}(1 - M_0 \cos\theta)\left[1 - 0.43\left(\frac{D_1 - 2H_1}{D_1}\right)^2\right]$$

$$\times \left\{1 + 0.62\left(\frac{V_1}{C_a}\right)\left[1 + \left(\frac{0.62\, V_1}{C_a}\right)^5\right]^{-1/5} \cos\theta\right\} \qquad (11a)$$

for the inner stream, and for the outer stream

$$f_{s,2}^{peak} = 0.62\, V_2/(2H_2) \Big/ \sqrt{M_2^2 - 1}(1 - M_0 \cos\theta)\left[1 - 0.43\left(\frac{D_2 - 2H_2}{D_2}\right)^2\right]$$

$$\times \left\{1 + 0.62\left(\frac{V_2}{C_a}\right)\left[1 + \left(\frac{0.62\, V_2}{C_a}\right)^5\right]^{-1/5} \cos\theta\right\} \qquad (11b)$$

The 1/3-octave-band SPL for each frequency is then obtained from figure 4. In figure 4 is shown the shock noise SPL for each 1/3-octave-band relative to the peak SPL as a function of the ratio of the 1/3-octave-band center frequency to the peak frequency.

### Incremental Effects

In addition to predicting absolute spectra, it is of interest to predict incremental changes. That is, given a set of experimental data, it is useful to predict the effect of changing a variable, such as free stream velocity or nozzle geometry. To do this a complete noise prediction is made for both cases: the case for which experimental data exist I and the unknown case II. The difference between these two cases $SPL_{II,\,pred} - SPL_{I,\,pred}$ is computed for each angle and frequency. This difference is then added to the experimental data for case I to generate an estimate of the noise for the unknown case $SPL_{I,\,exp} + (SPL_{II,\,pred} - SPL_{I,\,pred})$. In several of the figures which follow, the absolute level and a level computed by this incremental process are both included.

## COMPARISON OF PREDICTION WITH EXPERIMENTAL DATA

The empirical model presented in the preceding section is compared with some typical model-scale experimental data (refs. 2, 3, and 10) in this section. These comparisons include both static and simulated flight cases and include some variation in model size (total equivalent diameters from 5.7 to 15.2 cm). These comparisons are made for cases where both streams are subsonic, where the outer stream is supersonic with the inner stream subsonic, and where both streams are supersonic. The cases considered cover a limited range of inner-to-outer stream area ratio variation and include both coaxial (without center plug) and coannular (with center plug) nozzles. The test conditions are given in detail in table I.

For each case the experimental data are compared with the prediction at four angular locations, one in the forward quadrant ($60^{o} \leq \theta_a \leq 75^{o}$), one at $\theta_a = 90^{o}$, and two in the rear quadrant ($\theta_a = 120^{o}$ and $140^{o}$). (The symbol $\theta_a$ indicates the apparent angle, taken relative to the center of the inner nozzle exit plane; the emission angle, $\theta$, is different for each source region as described in appendix B.)

Some of the experimental data exhibit anomalous trends at very high frequencies, which may be due to incorrect atmospheric absorption corrections and/or data system inadequacies. Therefore, the data in the frequency range exhibiting anomalous trends (which is facility dependent) are not included in the plots. Since the experimental models were of rather small size, the very low frequencies (below about 20 Hz for a typical full scale engine) are also not included. The comparisons are made either on a lossless basis (corrected for atmospheric absorption) or corrected to standard day conditions.

## Both Streams Subsonic

Comparisons for a typical case with both streams subsonic are shown in figure 5. The nozzle is coaxial and noncoplanar with an area ratio, $A_2/A_1$, of 0.75 (ref. 2). The predicted premerged noise is shown by the dashed line, the predicted merged noise by the dash-dot line, and the total noise by the solid line. The predicted total noise, SPL (eq. (1)), is in good agreement with the experimental data in both level and spectral shape at $60^{o}$, $90^{o}$, and $120^{o}$. At $\theta_a = 140^{o}$ there is some overprediction at the middle frequencies although the high and low frequency regions are predicted well. However, there is no systematic trend apparent. Improvements in the spectra at aft angles ($\theta_a \geq 140^{o}$) may require some changes in the circular jet noise spectra.

### Both Streams Supersonic

Comparisons for a typical case with both streams supersonic are shown in figure 6; the nozzle is the same as for figure 5. All four individual noise components (premerged, merged, inner-stream shock, and outer-stream shock) are shown as well as the total. The predicted total noise is in reasonable agreement with the experimental data in level and spectral shape in the rear quadrant. At $75^{\circ}$ and $90^{\circ}$ there is a trend to overpredict the peak-SPL frequency, which is due to the inner-stream shock noise. This may be due to not accounting for shock interactions between the two streams, but even so the general agreement is reasonable.

### Outer Stream Supersonic with Inner Stream Subsonic

The remaining comparisons herein are for cases with the outer stream supersonic and the inner stream subsonic; such conditions are typical of a duct-burning turbofan cycle.

Effect of area ratio. - In figure 7 the comparison of experimental and predicted noise for the same 0.75-area ratio coaxial nozzle (same nozzle as in figs. 5-6) is shown, while in figure 8 similar comparisons are shown for a 1.2-area-ratio coaxial nozzle of the same total area at the same conditions (ref. 2). The agreement in the aft quadrant is reasonably good with the discrepancies small except at high frequencies, as previously noted. As was the case for the inner-stream shock noise in figure 6, there is an apparent overprediction of the peak-SPL frequency for the outer-stream shock noise. Because of the higher pressure ratio involved in the present case, the errors are more significant than in figure 6, but errors of this type would not have a serious effect on the perceived noise levels of a full-scale engine. In addition to the predicted total noise, figure 8 also shows a noise level calculated by applying the predicted configuration increment at each frequency, as discussed earlier

herein, to the experimental data for the 0.75-area-ratio nozzle (fig. 7). It can be seen that, except at 120°, the effect of area-ratio change is predicted even more accurately than the absolute level for the middle and low frequencies. At high frequencies the absolute prediction appears to be more accurate, probably because of scatter in the high frequency experimental data between the two cases.

Effect of simulated flight. - Figure 9 shows a comparison of experimental and predicted noise at near static ($M_a = 0.027$) conditions, while figure 10 shows similar comparisons for the same conditions except that the simulated flight Mach number, $M_a$, is 0.18.[2] (From ref. 10; the nozzle is geometrically similar to the 0.75-area-ratio nozzle of figs. 5-7, but is smaller in size.) The agreement of the static data with prediction is generally good. The agreement of these static data at reduced scale (about 0.4 times that of ref. 2) indicates the validity of the model for predicting the effects of size. For the simulated flight case the agreement is not quite as good, but the peak levels and spectral shapes are adequate for predicting perceived noise levels. In addition to the predicted total noise, figure 10 also shows a noise level calculated by applying the predicted flight increment at each frequency to the experimental data at near static conditions (fig. 9). There is a slight but consistent trend to underpredict the simulated flight noise.

Effect of inner-stream plug. - In figure 11 a comparison of experimental and predicted noise is shown for a 0.65-area-ratio coaxial, coplanar ($L_2 = 0$) nozzle, while in figure 12 similar comparisons are shown for a coannular plug nozzle of the same area ratio and total area at the same conditions (ref. 3). The source-to-microphone distance is greater than for the data in the previous figures; although this minimizes the source location corrections,

[2]The data have been Doppler frequency shifted to a flight frame of reference in ref. 10.

it increases the high-frequency experimental data problems. So as not to place undue emphasis on the high frequency problems, figures 11 and 12 are presented on a standard-day basis.[3] The absolute agreement for both configurations is marginal in some cases, but the spectral shapes are predicted well. To investigate the effect of the plug on a relative basis, figure 12 also shows a noise level calculated by applying the predicted configuration increment at each frequency to the experimental data for the coaxial (no plug) case (fig. 11). The agreement of these adjusted values with the experimental data is somewhat better than for the absolute prediction, indicating that the model properly predicts the effect of an inner-stream plug.

## CONCLUDING REMARKS

An empirical model is presented for predicting the noise from inverted-velocity profile coaxial and coannular jets, including the effects of flight. Comparisons of noise levels predicted by this model with model-scale experimental data indicate reasonable agreement. The incremental effects of changes in scale size, outer-stream to inner-stream area ratio, presence of an inner-stream plug, and simulated flight are shown to be generally predicted even more accurately than the absolute levels. Areas of potential improvement do exist, however, e.g., improvements in the circular jet noise prediction on which this method is based might produce even more accurate predictions. Inconsistencies in the experimental data at high frequency make it difficult to confidently assess the accuracy of the shock noise predictions, but it appears

---

[3]The experimental data are corrected to standard day (298 K, 70 percent relative humidity) atmospheric absorption and to free field conditions by methods of ref. 3. The predicted data are free field and are corrected to standard day atmospheric absorption by the method of ref. 12.

that some improvements, such as accounting for shock interactions between the two streams, should be considered.

The model presented herein is shown to give reasonable predictions of absolute noise spectra and even better predictions of incremental changes. This evidence indicates the basic soundness of the approach, i. e., the consideration of the various source regions and the fairly simple relations between the noise generating mechanisms and those of circular jets. The similarity of inverted-velocity-profile jets to circular jets in noise generating characteristics should eliminate the need for any ad hoc "data-fit" type approach to predicting inverted-velocity-profile jet noise.

# APPENDIX A

## SYMBOLS

| | |
|---|---|
| A | fully-expanded area, $m^2$ |
| D | inner diameter, m |
| f | 1/3-octave-band center frequency, Hz |
| H | gap height (radius for circular nozzle), m |
| $L_2$ | spacing of inner nozzle exit plane downstream of outer nozzle exit plane, m |
| M | fully-expanded Mach number, dimensionless |
| OASPL | overall sound pressure level, dB re 20 $\mu N/m^2$ |
| P | pressure, $N/m^2$ |
| PNL | perceived noise level, PNdB |
| R | source-to-observer distance, m |
| $R_a$ | distance from center of inner nozzle exit plane to observer, m |
| SPL | 1/3-octave-band sound pressure level, dB re 20 $\mu N/m^2$ |
| T | total temperature, K |
| V | velocity, m/sec |
| X | source position downstream of inner nozzle exit plane, m |
| $\beta$ | circular jet shock noise parameter, $\sqrt{M_j^2 - 1}$, dimensionless |
| $\theta$ | noise emission angle from source (relative to nozzle inlet axis), deg |
| $\theta_a$ | apparent noise emission angle from center of inner nozzle exit plane, deg |

Subscripts:

| | |
|---|---|
| a | ambient |
| exp | experimental |
| f | flight |
| j | circular jet |
| m | merged region |
| p | premerged region |
| P1 | plug nozzle |
| pred | predicted |
| s | shock noise |
| st | static |
| 0 | aircraft |
| 1 | inner stream |
| 2 | outer stream |
| I, II | sets of conditions |

Superscript:

| | |
|---|---|
| peak | highest shock noise level at a given angle |

# APPENDIX B

## SOURCE LOCATION CORRECTIONS

Experimental noise measurements are often made at a distance far enough away to be in the far field of any individual noise source region, but not far enough away to treat the entire exhaust plume as a point source. When this is the case, the prediction for each source must take into account the location of that source. This appendix gives the methods used herein to approximate these source location effects. The geometric relations for noise sources downstream of a nozzle exit are given in figure B1.

### Jet-Mixing Regions

The relations for the jet-mixing source regions are based very loosely on the conical nozzle data of reference 11. Figure B2 shows some samples of the angular and distance corrections for a circular jet with source position given by $X = (4 + \theta_a/90)D$.

Merged region. - The source position used in determining the far-field angles and distance for the merged-jet/ambient mixing region is given by

$$X_m = (4 + \theta_a/90)D_m \tag{B1}$$

This is an approximation to the source position where the peak-frequency noise at the angle of interest is generated. The variation of source position with frequency is not given explicitly, but is included to some degree of approximation in the spectral shapes.

Premerged region. - In a manner analogous to that used for the merged region, the source positions for the premerged-jet/ambient mixing region are given by

$$X_p = 2H_2(4 + \theta_a/90) - L_2 \tag{B2}$$

## Shock Noises

The relations used for the shock/turbulence interaction source regions have some foundation in the circular jet theory of reference 7. Reference 7 indicates that the first shock occurs at about 1.31 $D_\beta$ and that the spacing is about 6 percent of that distance. Furthermore, reference 7 indicates that about eight shocks are significant in the noise generation process. The approximation used here that the source position is at 1.5 $D_\beta$ (for a circular nozzle) emphasizes the earlier stronger shocks.

Inner-stream. - The source location for inner-stream shock/turbulence interaction noise is calculated from

$$X_{s,1} = 3H_1\left[1 - 0.43\left(\frac{D_1 - 2H_1}{D_1}\right)^2\right]\sqrt{M_1^2 - 1} \qquad \text{(B3)}$$

Outer-stream. - The source location for outer-stream shock/turbulence interaction noise is calculated from

$$X_{s,2} = 3H_2\left[1 - 0.43\left(\frac{D_2 - 2H_2}{D_2}\right)^2\right]\sqrt{M_1^2 - 1} - L_2 \qquad \text{(B4)}$$

## REFERENCES


1. E. Willis, "Variable-Cycle Engines for Supersonic Cruise Aircraft," Variable Geometry and Multicycle Engines, AGARD Conf. Proc. No. 205 (1976), Paper No. 7.

2. H. Kozlowski and A. B. Packman, "Aerodynamic and Acoustic Tests of Duct-Burning Turbofan Exhaust Nozzle," NASA CR-2628 (1976).

3. P. R. Knott, P. H. Heck, D. Latham, J. F. Brausch, E. J. Stringas, and P. S. Staid, "Acoustic Tests of Duct-Burning Turbofan Jet Noise Simulation," NASA CR-

4. O. A. Gutierrez, "Aeroacoustic Studies of Coannular Nozzles Suitable for Supersonic Cruise Aircraft Applications," Proceedings of the SCAR Conference, Part 2, NASA CP-001-PT-2, 471-490 (1976).

5. A. B. Packman, H. Kozlowski, and O. Gutierrez, "Jet Noise Characteristics of Unsuppressed Duct Burning Turbofan Exhaust System," J. Aircr. 14 (3), 227-232 (1977).

6. J. R. Stone, "Interim Prediction Method for Jet Noise," NASA TM X-71618 (1974).

7. M. Harper-Bourne and M. J. Fisher, "The Noise from Shock Waves in Supersonic Jets," Noise Mechanisms, AGARD Conf. Proc. No. 131 (1974), Paper No. 11.

8. D S. Dosanjh, P. K. Bhutiani, and K. K. Ahuja, "Supersonic Jet-Noise Reduction by Coaxial Cold/Heated Jet Flows," Syracuse University, Dept Mechanical and Aerospace Engineering, Final Report, Grant No. DOT-OS-20094 (March 1977).

9. R. E. Motsinger and A. R. Sieckman, "Prediction of Supersonic Jet Noise Reduction Using Multitube Nozzle Suppressors," General Electric Aircraft Engine Group Report No. R73AEG156 (1973).

10. H. Kozlowski and A. B. Packman, "Flight Effects on the Aero/Acoustic Characteristics of Inverted-Velocity-Profile Coannular Nozzles, Comprehensive Data Report," NASA CR-135189 ( ).

11. C. L. Jaeck, "Static and Wind Tunnel Near-Field/Far-Field Jet Noise Measurements from Model Scale Single-Flow Baseline and Suppressor Nozzles. Vol. I: Noise Source Locations and Extrapolation of Static Free-Field Jet Noise Data," NASA CR-137913 (Sept. 1976).

12. F. D. Shields and H. E. Bass, "Atmospheric Absorption of High Frequency Noise and Application to Fractional-Octave Bands," NASA CR-2760 (1977).

E9425

TABLE I. - TEST CONDITIONS FOR EXPERIMENTAL DATA

| Figure | Reference | Nozzle type (area ratio) | Inner stream | | | | | Outer stream | | | | | | Ambient | | | |
|---|---|---|---|---|---|---|---|---|---|---|---|---|---|---|---|---|---|
| | | | Velocity, $V_1$, m/sec | Temperature, $T_1$, K | Pressure ratio | Area, $A_1$, $cm^2$ | Hydraulic diameter, $2H_1$, cm | Velocity, $V_2$, m/sec | Temperature, $T_2$, K | Pressure ratio | Area, $A_2$, $cm^2$ | Hydraulic diameter, $2H_2$, cm | Spacing, $L_2$, cm | Apparent distribution, $R_a$, m | Stream velocity, $V_a$, m/sec | Temperature, $T_a$, K | Pressure, $P_a$, $kN/m^2$ |
| 5 | 2 | Coaxial (0.75) | 407 | 697 | 1.55 | 72.26 | 9.6 | 583 | 1083 | 1.80 | 54.19 | 2.88 | 3.3 | 4.57 | 0 | 302 | 101 |
| 6 | ↓ | ↓ ↓ | 611 | 812 | 2.45 | ↓ | ↓ | 716 | 1093 | 2.48 | ↓ | ↓ | ↓ | ↓ | ↓ | 301 | ↓ |
| 7 | ↓ | ↓ ↓ | 400 | 714 | 1.51 | ↓ | ↓ | 870 | 1101 | 4.11 | ↓ | ↓ | ↓ | ↓ | ↓ | 301 | ↓ |
| 8 | ↓ | ↓ (1.20) | 441 | 844 | 1.53 | 57.48 | 8.5 | 859 | 1081 | 4.06 | 68.97 | 3.84 | ↓ | ↓ | ↓ | 296 | ↓ |
| 9 | 3 | ↓ ( .75) | 296 | 389 | 1.52 | 14.32 | 4.3 | 575 | 707 | 2.51 | 10.77 | 1.26 | 1.7 | 3.05 | 9 | 298 | ↓ |
| 10 | 3 | ↓ ( .75) | 301 | 402 | 1.52 | 14.32 | 4.3 | 573 | 702 | 2.51 | 10.77 | 1.26 | 1.7 | 3.05 | 62 | 298 | ↓ |
| 11 | 10 | ↓ ( .65) | 357 | 553 | 1.57 | 109.1 | 11.8 | 548 | 664 | 2.42 | 70.66 | 3.26 | 0 | 12.19 | 0 | 284 | 100 |
| 12 | 10 | Coannular ( .65) | 374 | 556 | 1.60 | 111.0 | 8.2 | 552 | 667 | 2.46 | 71.38 | 2.17 | 8.3 | 12.19 | 0 | 286 | 100 |

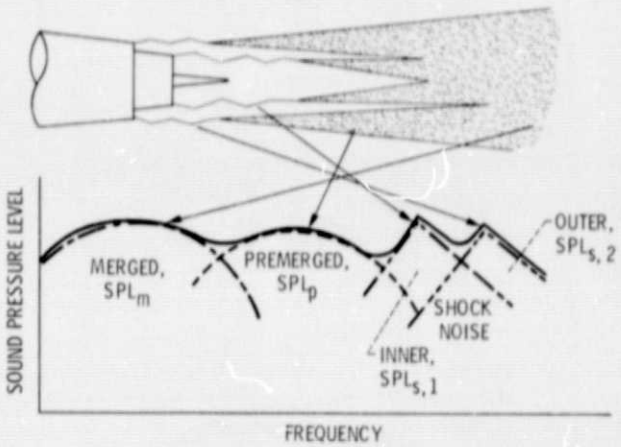


Figure 1. - Inverted-velocity-profile jet noise sources.



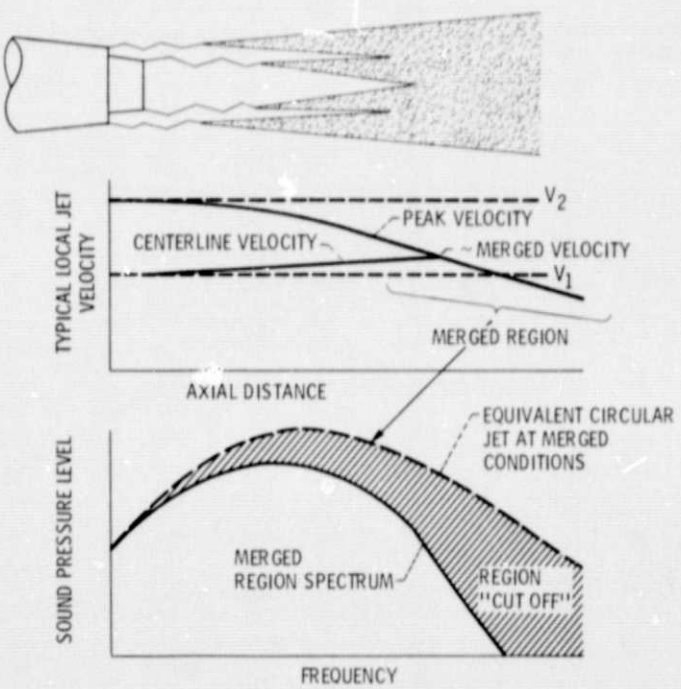


Figure 2. - Modeling of merged region noise generation for an inverted-velocity-profile coaxial jet.

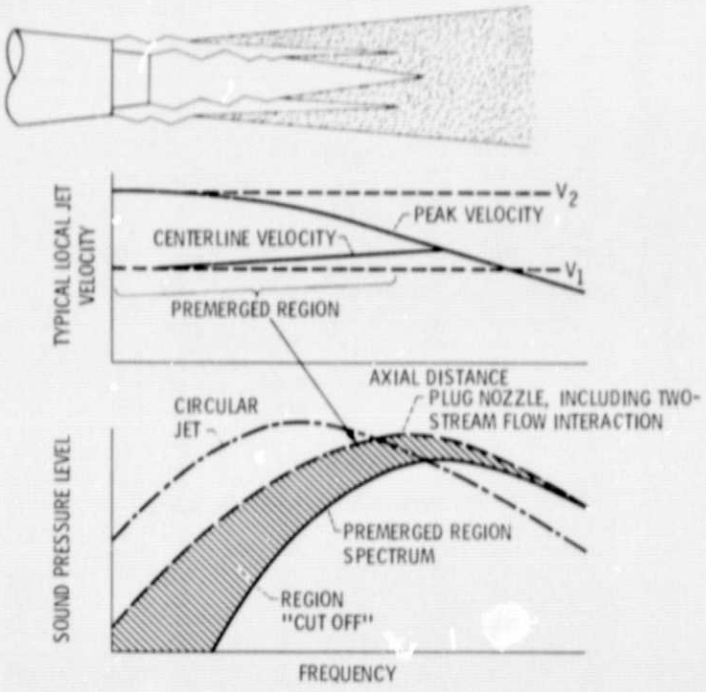


Figure 3. - Modeling of premerged region noise generation for an inverted-velocity-profile coaxial jet.

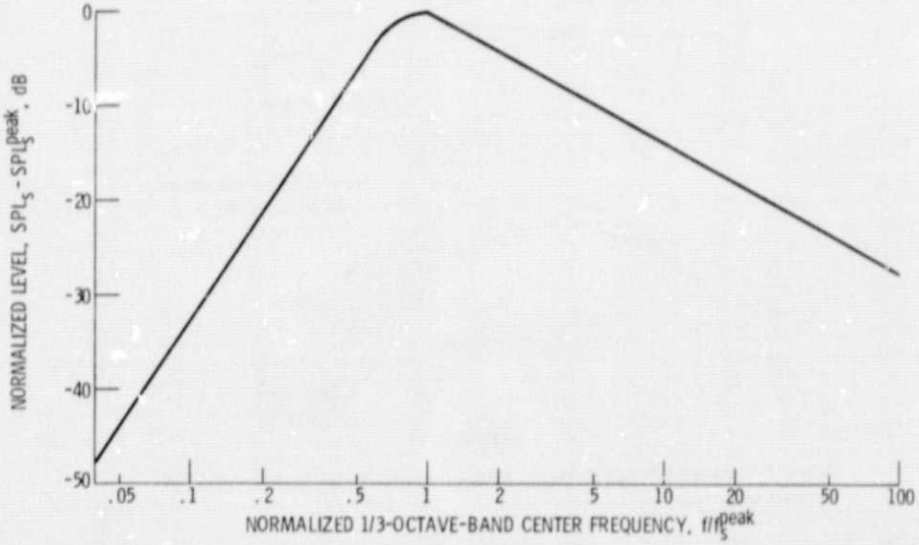


Figure 4. - Normalized shock noise spectra.

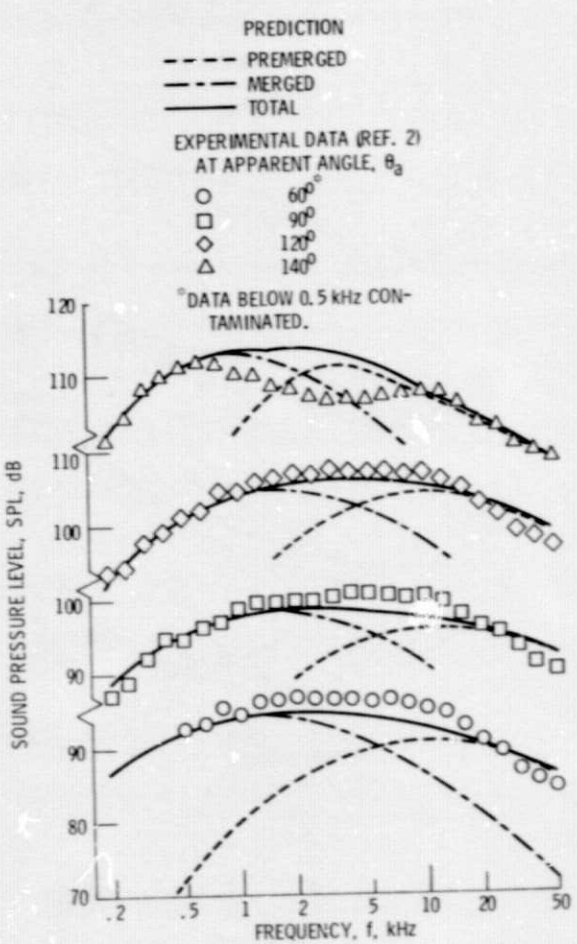


Figure 5. - Comparison of experimental and predicted spectra for 0.75-area-ratio coaxial, non-coplanar nozzle with both streams subsonic.

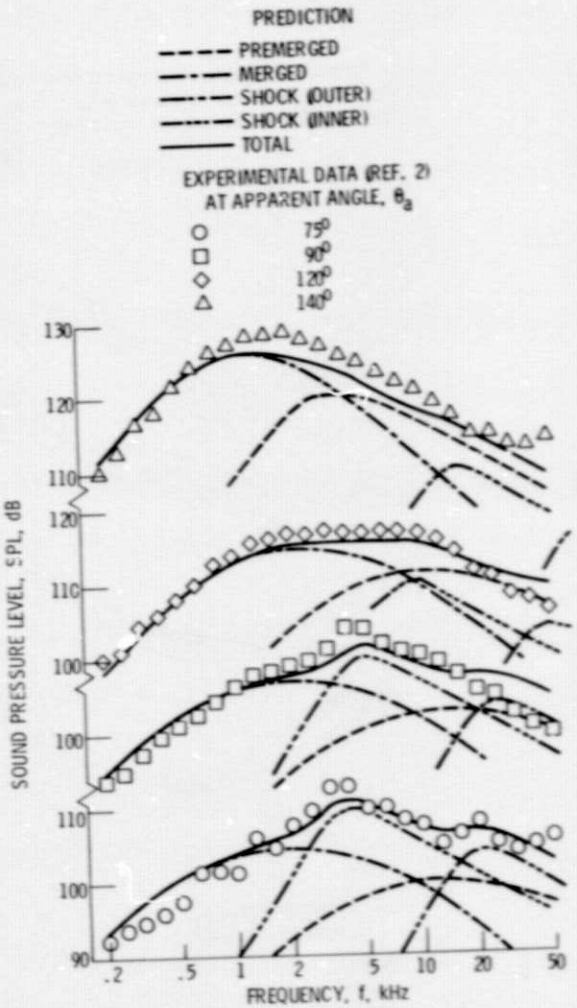


Figure 6. - Comparison of experimental and predicted spectra for 0.75-area-ratio coaxial nozzle with both streams supersonic.

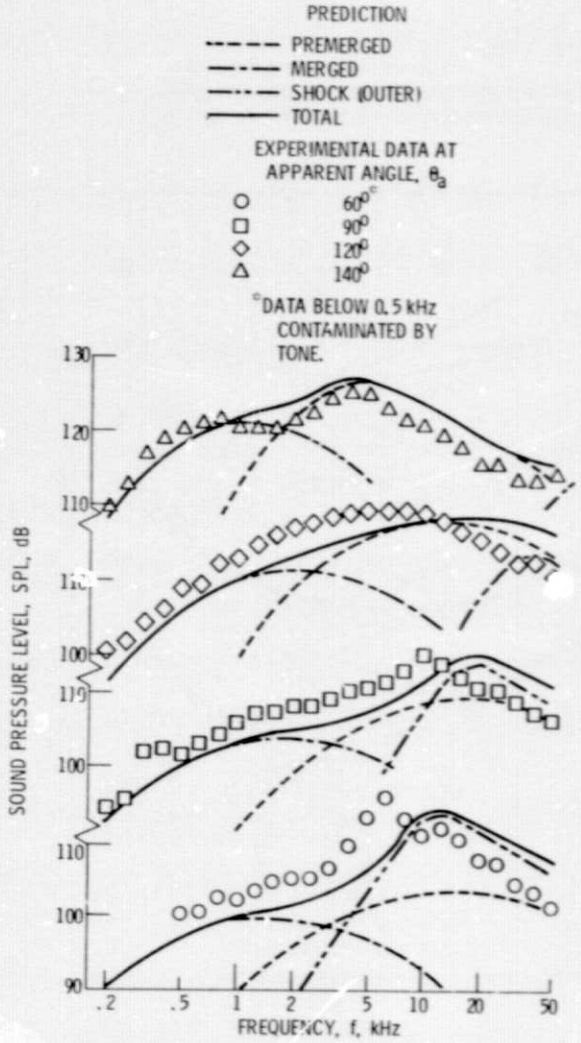


Figure 7. - Comparison of experimental and predicted spectra for 0.75-area-ratio coaxial nozzle with inner stream subsonic and outer stream supersonic.

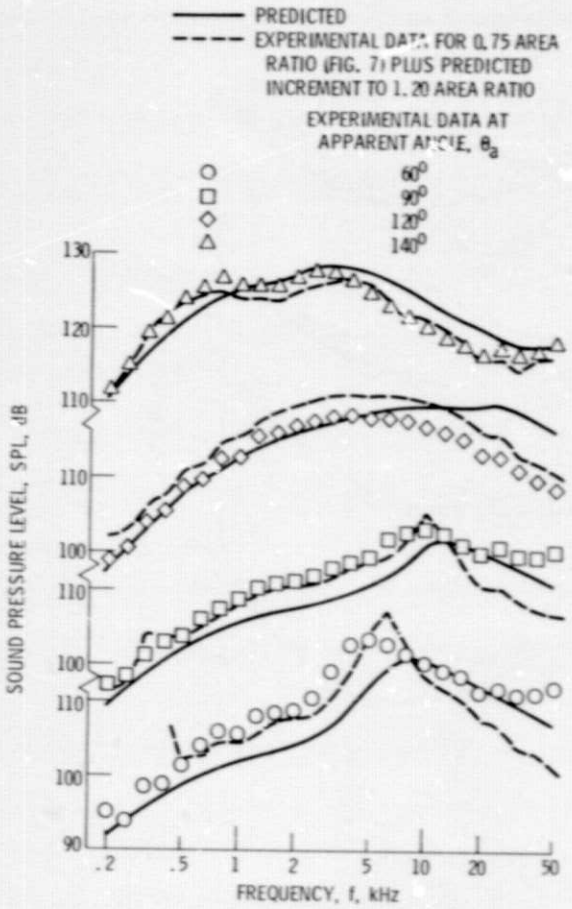


Figure 8. - Comparison of experimental and predicted spectra for 1.20-area-ratio coaxial nozzle with inner stream subsonic and outer stream supersonic.

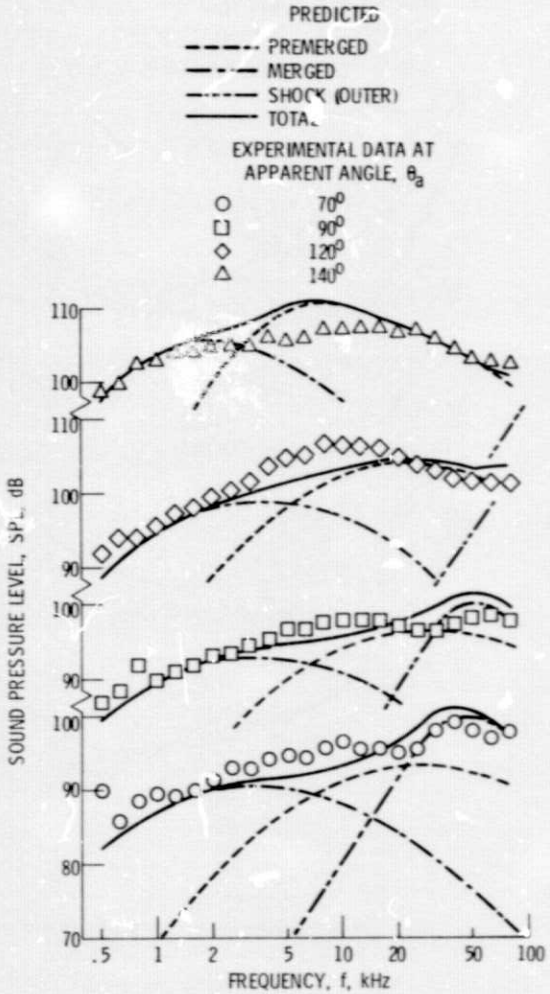


Figure 9. - Comparison of experimental and predicted spectra for 0.75-area-ratio coaxial nozzle with inner stream subsonic and outer stream supersonic at near-static conditions ($M_a$ = 0.027).

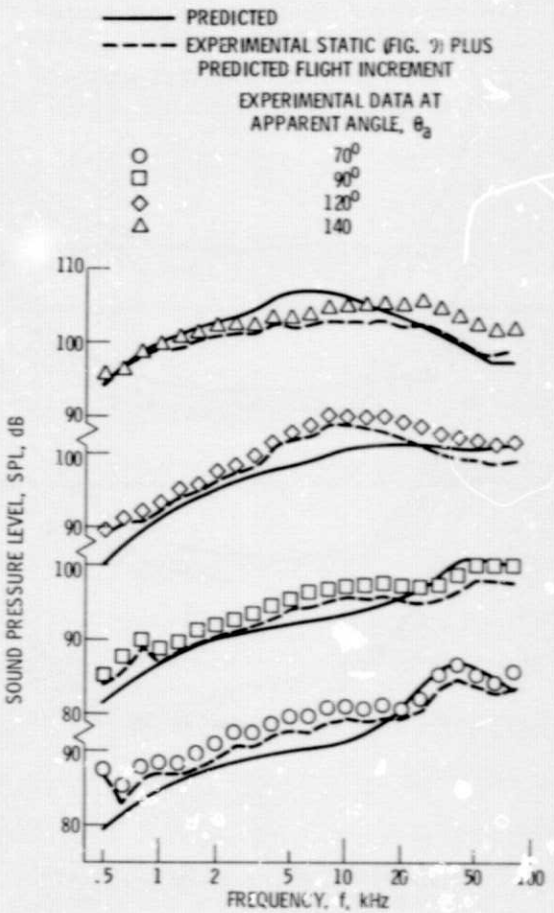


Figure 10. - Comparison of experimental and predicted spectra for 0.75-area-ratio coaxial nozzle with inner stream subsonic and outer stream supersonic in simulated flight at $M_a$ = 0.18.

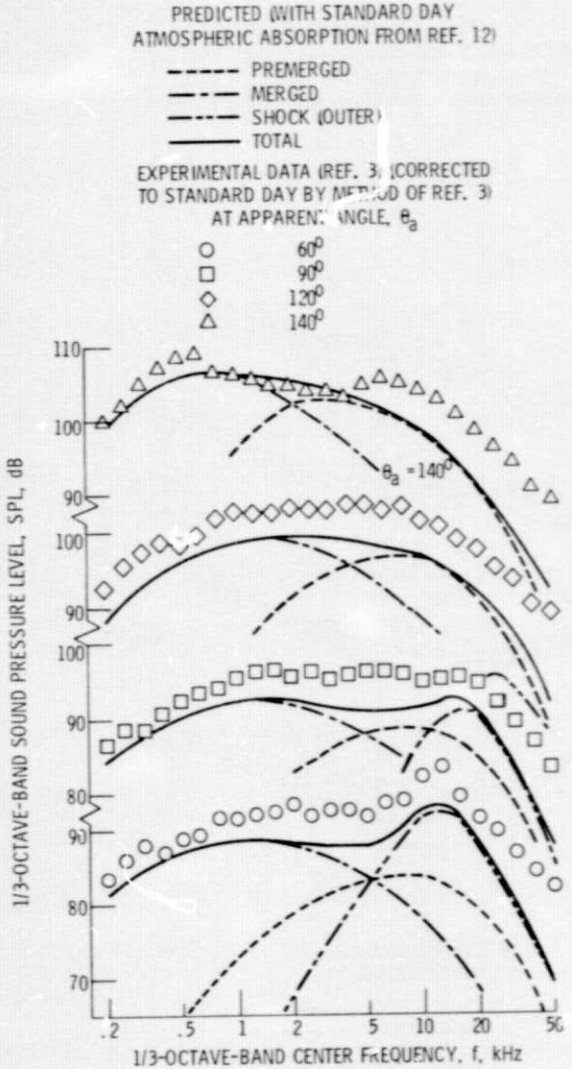


Figure 11. - Comparison of experimental and predicted spectra for 0.65-area ratio coaxial, coplanar nozzle with inner stream subsonic and outer stream supersonic.

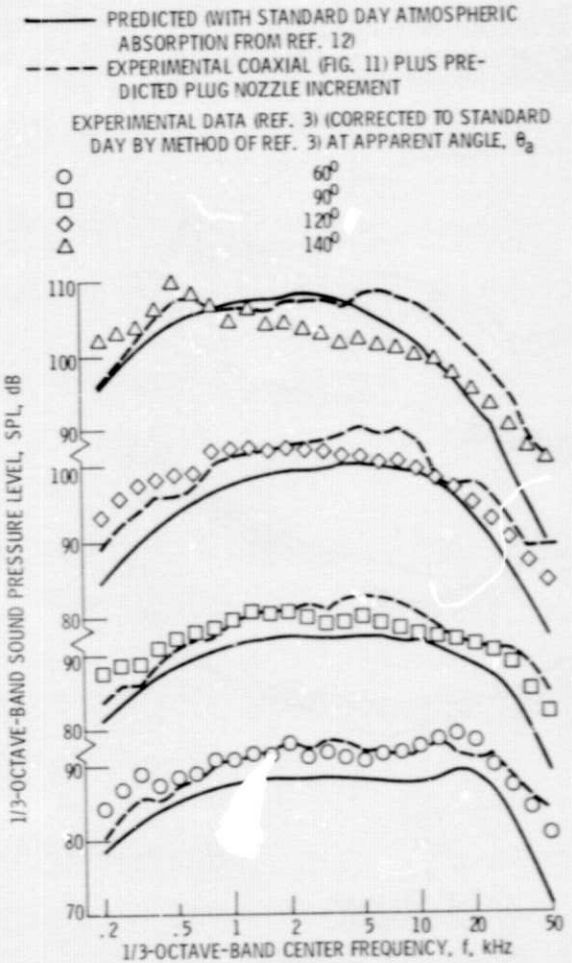


Figure 12. - Comparison of experimental and predicted spectra for 0.65-area ratio coannular plug nozzle with inner stream subsonic and outer stream subsonic.

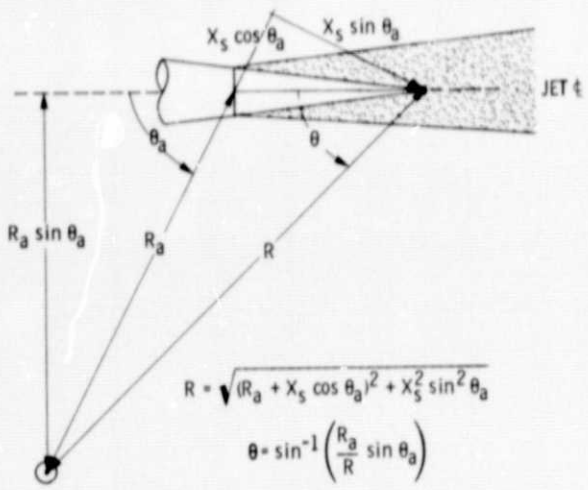


Figure B1. - Geometric relations for jet noise source located downstream of nozzle exit plane.



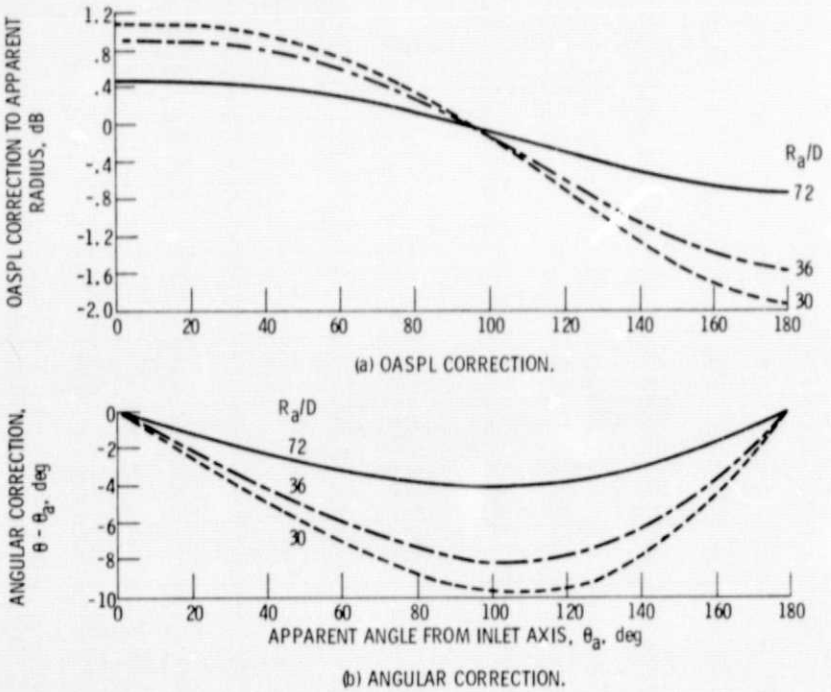


Figure B2. - Corrections to be applied to jet noise data taken at constant apparent radius.

NASA-Lewis